Journal of the Korean Nuclear Society
Volume 32, Number 1, pp.17~33, February 2000

A Mechanistic Critical Heat Flux Model for High-Subcooling, High-Mass-Flux, and Small-Tube-Diameter Conditions

Young Min Kwon
Korea Atomic Energy Research Institute
150 Dukjin-dong Yusong-gu, Taejon 305-353, Korea
ymkwon@kaeri.re.kr

Soon Heung Chang
Department of Nuclear Engineering
Korea Advanced Institute of Science and Technology
373-1, Kusong-dong, Yusong-gu, Taejon, 305-701, Korea
(Received July 26, 1999)

Abstract

A mechanistic model based on wall-attached bubble coalescence, previously developed by the authors, was extended to predict a very high critical heat flux (CHF) in highly subcooled flow boiling, especially for high mass flux and small tube diameter conditions. In order to take into account the enhanced condensation due to high subcooling and high mass velocity in small diameter tubes, a mechanistic approach was adopted to evaluate the non-equilibrium flow quality and void fraction in the subcooled water flow boiling, with preserving the structure of the previous CHF model. Comparison of the model predictions against highly subcooled water CHF data showed relatively good agreement over a wide range of parameters. The significance of the proposed CHF model lies in its generality in applying over the entire subcooled flow boiling regime including the operating conditions of fission and fusion reactors.

Key Words : critical heat flux (CHF), mechanistic model, subcooled flow boiling

1. Introduction

The subcooled flow boiling of water has been recognized as a very effective cooling mode due to its enhanced heat transfer mechanism. In studies of subcooled flow boiling, much effort has been devoted to the critical heat flux (CHF), because CHF is one of the most important considerations in the design and safety analysis of nuclear reactors. The cooling system should be operated to maintain the heated wall below the CHF condition to avoid the risk of physical burnout. For the thermal hydraulic design of light water reactors (LWRs), the magnitude of heat fluxes is generally on the order of 1 MW/m^2. However fusion reactor components require a very high heat removal rate, an order of magnitude higher than LWRs. In high-heat-flux systems, thermal

management by appropriate cooling is one of the engineering problems to be resolved.

In order to understand the physical nature of the CHF phenomenon, various phenomenological models based on the CHF mechanism have been developed. The mechanistic models have advantage, with respect to other CHF prediction methods, that it would be easily improved and extended to a wide range of operating conditions by modifying the relevant constitutive models. The bubble crowding model [1] and the liquid sublayer dryout model [2, 3] are receiving considerable attention for prediction of CHF; however, these models were mainly based on the operating conditions of LWRs. Assessments of models and correlations by Celata et al. [4] and Inasaka and Nariai [5] have shown that the existing prediction methods, developed for LWR operating conditions, could not be recommended for application to fusion reactor components.

The authors believe that the near-wall flow structure at the CHF condition does not significantly depend on the subcooling degree from the standpoint of CHF mechanism. Since no existing mechanistic model is applicable for both LWRs and fusion reactors while keeping reliable prediction performance, it is desirable to have a general predictive procedure that applies to a wide range of operating conditions.

Kwon and Chang [6] have developed a new CHF model based on the concept of wall-attached bubble coalescence and demonstrated their model could predict CHF in a wide range of flow conditions, including subcooled and low quality conditions. The model was capable of predicting the CHF of non-aqueous fluids (Freon-12 and 113) with reasonable accuracy [7]. The objective of this paper is to evaluate the prediction performance of the authors' previous model for high-heat-flux applications such as fusion reactors. An attempt of extension was made by adopting a mechanistic approach to calculate the profiles of non-equilibrium flow quality and void fraction under high subcooling and high mass flux conditions, while preserving the structure of the previous model. A brief summary of the previous model developed by the authors [6, 7] is presented in the following section.

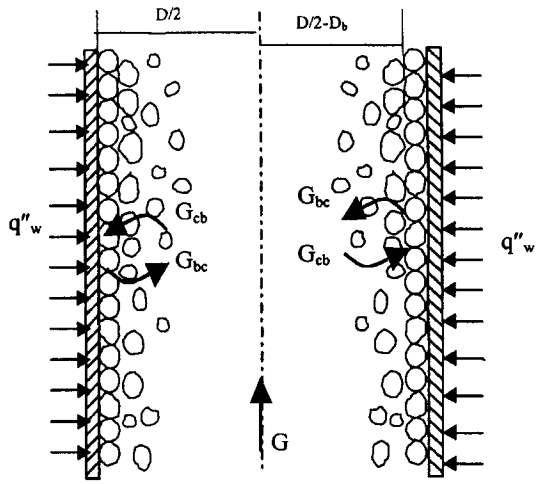

Fig. 1. Conceptual Configuration of Bubbles on the Heated Wall

2. CHF Model Based on Wall-Attached Bubble Coalescence

A physical image of the boiling structure considered is shown in Fig. 1, where the transverse interchange crossing the interface of the wall bubbly layer and core is shown. In the outer annular layer of the round tube, attached bubbles are packed on the wall just prior to agglomeration, and in the middle of the tube is a mixture core consisting of liquid and bubbles. The effective thickness of the bubbly layer is considered as a single bubble diameter, because it is assumed that only the wall-attached bubbles are responsible for the effective physical barrier to the heat

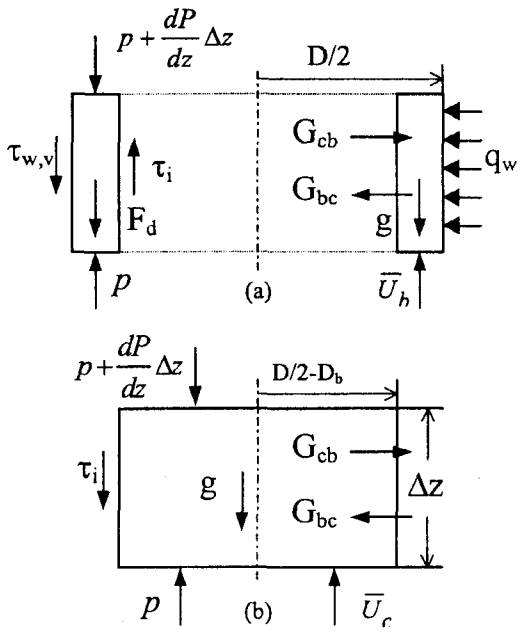

Fig. 2. Separated Flow Control Volumes for (a) Wall Bubbly Layer and (b) Core

transfer from the wall and the liquid supply from the core.

According to Saha and Zuber [8], at high mass flow rates, bubbles do not easily detach from their nucleation sites because small bubbles resist detachment from the wall by hydrodynamic forces. Therefore, the wall-attached bubbles form a wall bubbly layer, which acts as a wall roughness, increasing the roughness of the tube. The existence of roughness changes the hydrodynamic characteristics of the flow and the drag force on the wall-attached bubbles depends upon the characteristic skin friction experienced by the wall bubbly layer. It is assumed that bubbles are packed in a most dense array on the wall near the CHF condition. Then, the CHF is assumed to occur at a certain void fraction in the wall bubbly layer (called a critical wall-void fraction) when radial thermal transport is limited by equal flows inward and outward at the interface of the wall bubbly layer and core.

Governing equations are derived by applying the basic local conservation rules for mass, energy, and momentum to the control volumes such as that shown in Fig. 2. From total mass and energy balances on the wall bubbly layer of Fig. 2(a), the CHF formula of Eq. (1) is derived.

$$q''_{CHF} = G^*(h_b - h_c)\frac{\xi_i}{\xi_w} \tag{1}$$

The parameter of G* is the limiting transverse interchange of mass flux at the interface of the wall bubbly layer and core, which is obtained from the momentum balance equations on the control volumes of the wall bubbly layer and core, respectively.

$$G^* = \left[-(\rho_c - \rho_b)g + \frac{\pi D F_d}{D_b^2(1-\eta_c)A}\right]\frac{A\eta_c(1-\eta_c)}{(\bar{U}_c - \bar{U}_b)\xi_i} \tag{2}$$

In Eq. (2), the frictional drag, F_d, defined as a force that a rough element of single bubble exerts on the flow field, is evaluated by relating it to the skin friction coefficient of wall-attached bubble roughness, as done by the Staub' s [9] subcooled boiling model. As a first approximation, the frictional drag is assumed to be $F_d \cong (\lambda\rho U_c^2/2)\times(\pi D_b^2/4)$. As CHF usually occurs at the end of the heated tube in the case of uniform heating, thermo-physical properties are defined at the tube exit with assumption of homogeneous flow.

The Levy [10] model is employed to predict the point of onset of bubble departure (OBD) and the bubble departure diameter. The turbulent skin friction coefficient λ is calculated using the Colebrook-White equation with a two-phase Reynolds number to account for the variation of the fluid viscosity near the heated wall. The average viscosity of the core is evaluated by Beattie and Whalley [11]. The universal velocity

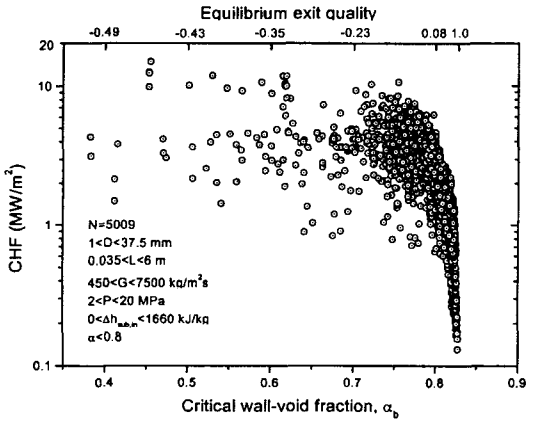

Fig. 3. CHF vs Critical Wall-Void Fraction

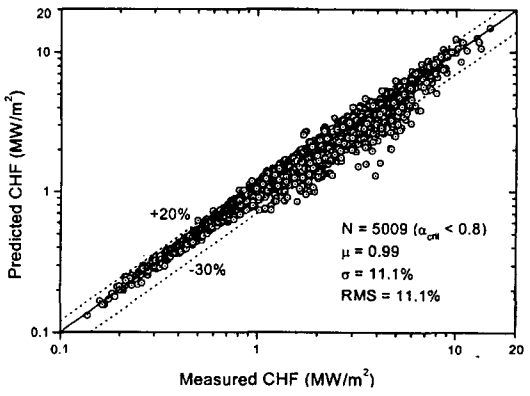

Fig. 4. Predicted to Measured CHF

profile for a single-phase turbulent flow proposed by Karman is assumed to be valid in the turbulent core. The average fluid velocity of the wall bubbly layer is determined by taking it as half the velocity of the core at the outer edge of the wall bubbly layer. The flow quality and void fraction in the subcooled flow boiling can be evaluated by the simple profile-fit method of Saha and Zuber [8] and Dix [12] model, respectively. All equations utilized in the present model are presented in Appendix I.

The critical wall-void fraction, α_b, was approximately correlated by the relation of Eq. (3) in the authors' previous work [6], which is only valid for $\alpha_{avg} \leq 0.8$.

$$\alpha_b = 0.83 - 0.29\exp(-4.71x_{em} - 1.89) \qquad (3)$$

Since the available void fraction in the bubbly layer near the CHF is quite limited experimentally and theoretically, the correlation was obtained by fitting against a total of 5009 data points. Assuming the validity of the functional forms of the constitutive relations employed in the CHF model, the choice of α_b in collaboration with available experimental CHF data was optimized. The parameter ranges of the experimental data are: $1 \leq D \leq 37.5$ mm, $0.035 \leq L \leq 6$ m, $450 \leq G \leq 7500$ kg/m^{2}s, $2 \leq P \leq 20$ MPa, and $0 \leq \Delta h_{sub,in} \leq 1660$ kJ/kg, most of which are in a low quality saturated condition. Only 902 out of 5009 data points belong to subcooled conditions at the tube exit. Fig. 3 shows the predicted CHF as a function of α_b, where the corresponding equilibrium quality, x_{em}, is presented in the top of the x-axis. The α_b decreases as the CHF increases, even though some scattered data exist. This trend is consistent with the experimental observation by Styrikovitch et al. [13] that the wall void fraction at the CHF dropped significantly at very high subcooling and high heat fluxes. Fig. 4 shows the visual comparison of the predicted and measured CHF using the above data set. Most of the experiment data (about 93%) were successfully predicted within a $\pm 20\%$ error band with the use of Eq. (3).

3. CHF Prediction for High-Subcooling, High-Mass-Flux, and Small-Tube-Diameter Conditions

According to Celata [14], the thermal hydraulic

conditions of fusion reactor components are high subcooling (up to 250 K), high mass flux (greater than 10 Mg/m^2s), small-intermediate tube diameter (1-15 mm), low-intermediate pressure (up to 5 MPa), and very high heat flux (up to 80 MW/m^2). The CHF under the condition of typical fusion reactor components may be different from that under the regular subcooled flow boiling condition. It has been recognized that highly subcooled flow boiling under conditions of high mass flux and small tube diameter can accommodate very high heat fluxes.

The authors' previous CHF model [6, 7], except for the following constitutive model, was utilized in this study. A mechanistic method to evaluate the non-equilibrium flow quality and void fraction in subcooled flow boiling was employed to take account of the enhanced condensation due to high subcooling in small diameter tubes.

3.1. CHF Model Modification

There are two distinctly different approaches to predict the flow quality and void fraction in the subcooled flow boiling; a profile-fit method and a mechanistic method. The profile-fit method is fully empirical, while the mechanistic method satisfies some conservation laws but still uses empirical relations for closure. The profile-fit method is easier to use than the mechanistic method. The mechanistic model may have insufficient data to accurately specify the basic mechanism involved, but it does afford a valid functional form of the basic physics involved. One of the important issues in developing an accurate mechanistic model for high subcooling and high mass velocity conditions is the accurate estimation of the condensation rate.

In the authors' previous CHF model, the flow quality was evaluated by the simple profile-fit model of Saha and Zuber [8], because little difference in the CHF predictions appeared for low subcooled and low quality conditions when both methods were employed. The relationship between the flow quality x_{avg} and the thermodynamic equilibrium qualities is expressed by Eq. (4).

$$x_{avg} = \frac{x_{em} - x_d \exp(x_{em}/x_d - 1)}{1 - x_d \exp(x_{em}/x_d - 1)} \tag{4}$$

where x_d and x_{em} are thermodynamic equilibrium qualities determined at the OBD point and at the tube exit, respectively. The location of the OBD is the most important parameter in Eq. (4), which is evaluated by the Levy [10] model.

For the high subcooled flow boiling with high mass flux and small diameter tubes, which is the focus of this paper, Nariai and Inasaka [15] reported that much lower void fraction was observed than the prediction by the profile-fit model. They considered that the difference in void fraction was caused by the intense condensation effect for the small diameter tubes with high liquid velocity. As tube inside diameter decreases and mass flow rate increases, the diameter of the bubbles generated on the wall becomes smaller due to the intense condensation effect by the transverse mixing mass flux of highly subcooled water. However, no satisfactory models for considering condensation in the extreme conditions of high subcooling, high liquid velocity and small diameter tubes actually exist at the present time, which is understandable in view of the complexity of the turbulence induced condensation process.

The mechanistic method to evaluate the flow quality and void fraction in the subcooled flow boiling was employed to take into account the enhanced condensation due to high subcooling in the small diameter tubes. In the subcooled flow boiling, the heat flux at the heating wall is typically partitioned into that required to generate vapor,

Table 1. Experimental CHF Data for Subcooled Flow Boiling

Parameter / Reference	No.	D (mm)	L (m)	P (MPa)	G (Mg/m^2s)	Δh_{in} (k_J/kg)	q''_{CHF} (MW/m^2)
Thompson et al.[20]*	541	1.14~37.5	0.04~1.97	2.14~19.0	0.66~7.5	49.0~1659	1.1~14.8
Becker et al. [21]*	114	6.0~10.0	0.4~3.0	3.04~20	0.37~6.98	587~1384	0.64~7.48
Zenkevich [22]*	245	5.8~11.0	1.0~4.0	7.85~19.6	0.96~5.06	239~1617	0.94~7.29
Chen et al. [23]	109	10.0~16.0	0.03~0.04	0.15~1.66	1.43~13.4	228~701	4.17~14.56
Boyd [24-26]**	28	10.2	0.5~1.17	0.45~1.6	0.76~7.45	544~772	1.39~11.5
Nariai et al. [27]	14	6.0	0.1	0.1~1.5	4.59~8.69	245~671	8.5~22.1
Celata et al. [3]	1887	0.33~2.54	0.002~0.61	0.09~8.4	0.93~90.0	88~1018	3.33~228
Total	2938	0.33~37.5	0.002~4.0	0.1~20.0	0.37~90.0	49.0~1659.0	0.64~228.0

* Data used for fitting of Eq.(3)

** Data not included in the ENEA database[3]

that associated with single-phase convection, and that due to liquid agitation or pumping. Rouhani and Axelsson [16] neglected the single-phase convection component based on the assumption that the heating wall was fully covered by bubbles downstream of the OBD point and considered the pumping component only. Then they modified the pumping factor, defined first by Bowring [17], in the form of Eq. (5).

$$\varepsilon' = \frac{\rho_l (h_f - h_l)}{\rho_g h_{fg}} \tag{5}$$

The resulting expression for true flow quality between the OBD and the interesting point along the heated flow path was given by Lahey and Moody [18]:

$$x_{avg} = \frac{1}{GAh_{fg}} \left\{ \int_a^z \frac{P_H q''_b dz}{[1+\varepsilon']} - \int_a^z P_H q''_{cond} dz \right\} \tag{6}$$

where P_H is the heated perimeter, and the net boiling heat flux q''_b is given by :

$$q''_b = q''_w \left\{ 1 - \left[\frac{h_f - h_l}{h_f - h_d} \right] \right\} \quad \text{for} \quad h_l \geq h_d$$
$$q''_b = 0 \quad \text{for} \quad h_l < h_d \tag{7}$$

As a first step for taking into account the condensation effect on the CHF, a first order model by Levenspiel [19] was used to test the physics of the condensation modeling.

$$q''_{cond} = 270 \frac{h_{fg} \rho_{fg}}{P_H} A \alpha_{avg} (T_{sat} - T_l) \quad \text{for} \quad h_l \geq h_d$$
$$q''_{cond} = 0 \quad \text{for} \quad h_l < h_d \tag{8}$$

where the constant value of 270 $(h\,^{\circ}C)^{-1}$ was fitted by the experimental void data by Levenspiel. An iterative approach is required to calculate x_{avg} at the tube exit, as shown in Appendix I. The detailed description of the prediction procedure is described in Lahey and

Moody [18].

3.2. Experimental CHF Data

Among the total of 5009 experimental CHF data used for the fitting of Eq. (3) in the previous works [6,7], only 902 data points [20-22] have a subcooled condition at the tube exit, most of which are categorized into a regular subcooled flow boiling condition. The high heat flux region for fusion reactor application is generally defined as the region where a heat flux is more than 10 MW/m^2.

In order to evaluate the proposed CHF predictive procedure, a total of 2938 CHF data points for water flow in uniformly heated round tubes was utilized. The ENEA CHF database in the range of fusion reactor thermal hydraulics was collected by Celata et al. [4]. The ENEA data set composed of 1887 data points was accumulated from twenty-five sources. Recent data sets of Chen et al. [23], Boyd [24-26], and Nariai et al. [27] were included in the present database. The data of Boyd were obtained from a horizontal tube test, but the effect of tube orientation was negligible because of the high mass flux. The range of parameters for each data source considered in this study is presented in Table 1. The parameter ranges are: $0.3 \leq D \leq 37.5$ mm, $0.002 \leq L \leq 4$ m, $0.1 \leq P \leq 20$ MPa, $0.37 \leq G \leq 90$ Mg/m^2s, $49 \leq \Delta h_{sub,in} \leq 1659$ kJ/kg, and $0.64 \leq q''_{CHF} \leq 228$ MW/m^2, which covers the operating ranges of typical fusion reactor components.

It was known that the subcooled convective boiling CHF is strongly affected by two parameters of mass velocity and subcooling (exit quality), and the effect of pressure is not explicitly shown in the low pressure range. Nariai and Inasaka [15] systematically investigated the effect of tube diameter and tube length on the CHF. Experiments were conducted at nearly ambient pressure under conditions: D = 1, 2, 3 mm; L = 1, 3, 5, 10 cm; G = 7000, 13000, 20000 kg/m^2s; inlet water temperature T_{in} = 20, 60 °C. The abnormality of the subcooled flow boiling in the narrow tubes with high mass flux was found. The actual void fraction for the narrow tubes with high liquid velocity became considerably different from those estimated by the existing correlations or models. Nariai and Inasaka reported that, for D = 1 mm and G = 13000 kg/m^2s, the estimated void fraction was about 70% of the theoretical prediction by the Ahmad model [28]. For D = 1 mm and G = 20000 kg/m^2s, the estimated void fraction was about 45% of the theoretical one. The reduced void fraction at the tube exit resulted in the increase of the CHF.

Ornatskii and Vinyarskii [29] obtained CHF higher than 200 MW/m^2 under the conditions of G = 90 Mg/m^2s, $P \approx 3$ MPa, $\Delta T_{sub,in} \approx 200$ K, D = 0.5 mm, and L = 14 mm. Their experimental data are included in the ENEA database [4]. The CHF mechanism under these extreme conditions may be largely different from those governed in the LWRs. As a first step, the present CHF database was simply classified into two categories based on the tube inside diameter and mass velocity. For most data satisfying $D < 3$ mm, since their mass velocities are relatively high comparable to the Nariai and Inasaka's [15] experimental condition, only the tube inside diameter was selected as the classification criterion for simplicity in this analysis. The first category dealing with the CHF data of $D < 3$ mm includes 1038 out of 2938 data points. Among them 246 data points have less than a 1 mm inside diameter. The second category of $D \geq 3$ mm includes the remaining 1900 data points. The D = 3 mm was obtained from the experiment by Nariaia and Inasaka. However, the actual value for this boundary could not be clarified in this initial

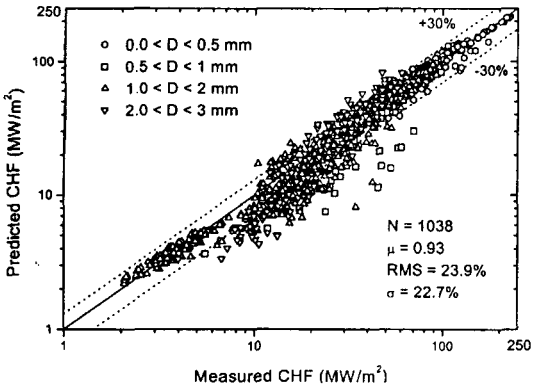

Fig. 5. Predicted vs Measured CHF for D <3mm

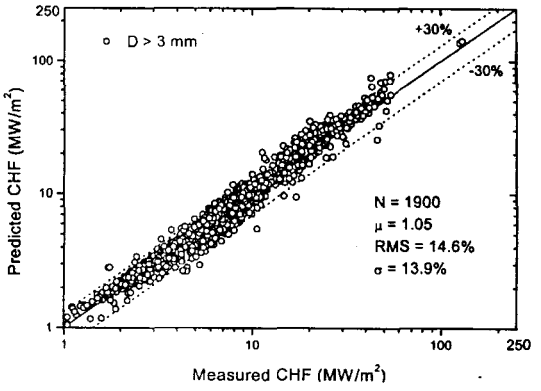

Fig. 6. Predicted vs Measured CHF for D ≥3mm

assessment and may be defined after further analysis.

It should be noted that we have tried to classify the CHF database following the guide of Inasaka and Nariai [5]. They divided their CHF database for high-heat-flux subcooled flow boiling into two regions based on the flow characteristics, but the criteria of the boundary between two regions were not clearly provided. The two regions are: the special parameter region (SPR) for high mass velocity with a small inside diameter and short length tube, and the normal parameter region (NPR) for the remaining case in the database. Inasaka and Nariai assumed that the CHF data belonged to SPR when $D < 3$ mm and $U_{avg} > 10$ m/s, or when L/D ≤ 50 and $U_{avg} > 20$ m/s. The remaining cases are NPR. In the present database, 776 data were categorized into SPR, and 2162 data were NPR. However, as a result, the predictions by the proposed model in the limited present database did not seem to be affected by the classification. There was no difference in the prediction performance in the two regions.

3.3. CHF Prediction by the Proposed Model

The calculation procedure is presented in Appendix I. The prediction performance of the CHF model was quantitatively evaluated by the CHFR, defined as the ratio of the predicted to measured CHF, with three statistical parameters of μ (average value), σ (sample standard deviation), and *RMS* (root-mean-square error) of the CHFR. The comparisons were conducted for two tube diameter ranges of $D < 3$ mm and $D \geq 3$ mm. Figs. 5 and 6 show the visual comparison of the predicted and measured CHF for each region, respectively, where the mechanistic method was employed in the prediction. The symbol N in the plots means the number of experimental data that was successfully predicted by the model. For small diameter tubes, the comparison results in Fig. 5 show a relatively large discrepancy, and the proposed model underestimated the CHF with $\mu = 0.93$, $RMS = 23.9\%$, and $\sigma = 22.7\%$. However, for the D $\geq$ 3 mm region, the proposed model predicted fairly well, as shown in Fig. 6, a most of the experiment data were predicted within a $\pm$ 30% error band with $\mu = 1.05$, $RMS = 14.6\%$, and $\sigma = 13.9\%$. It should be noted that, for some data points in the ENEA data set, the mechanistic flow quality model predicted higher average bulk void fraction larger than 0.8 at the tube exit. As is known, the prediction accuracy by the proposed

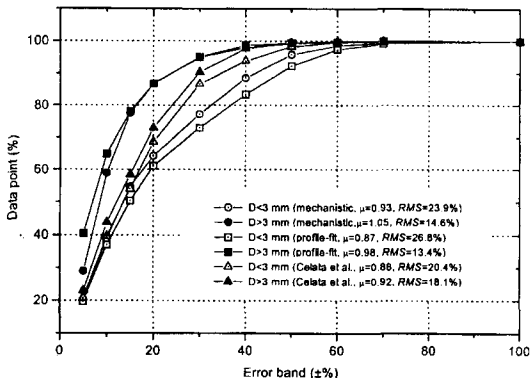

Fig. 7. Percentage of Data Points Predicted Within Error Band by the Proposed and Celata et al. Models

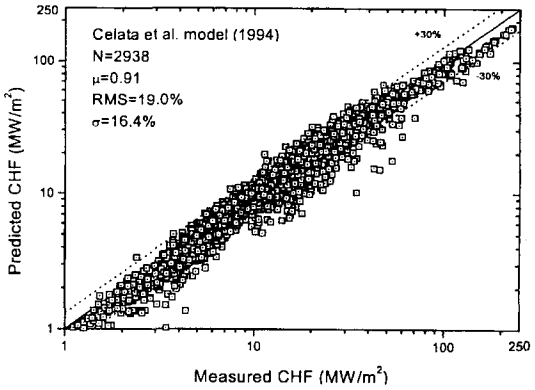

Fig. 8. CHF Predictions by the Celata et al. Model

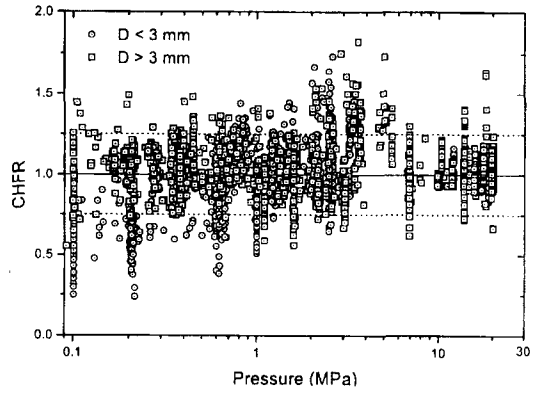

Fig. 9. CHFR vs Pressure

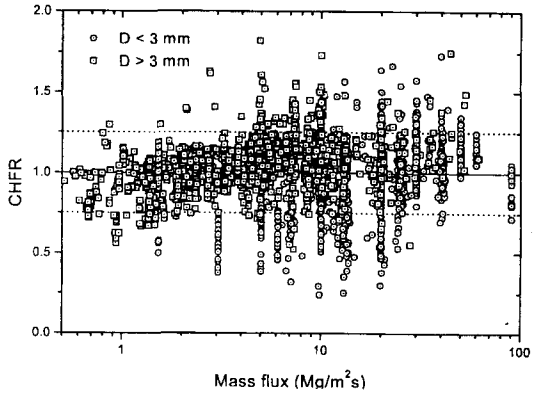

Fig. 10. CHFR vs Mass Flux

CHF model deteriorates when the average void fraction exceeds 0.8.

The percentage of data points calculated with the corresponding error band ($\pm$%) is presented in Fig. 7. The effects of the flow quality model in subcooled convective boiling for both regions are shown in the figure. Generally, the mechanistic method predicted higher CHF than the profile-fit method. Especially for small diameter tubes the profile-fit method gave greater underestimated values (μ = 0.87). The mechanistic method results were better than the profile-fit results for this region. This is mainly a consequence of a large condensation effect. For the D $\geq$ 3 mm region, even though no considerable difference in the prediction results between the two methods was shown in Fig. 7, the profile-fit method results were slightly better than the other ones. The prediction results by the Celata et al. model are included in the same figure. The Celata et al. model gave the most reasonable predictions for a small tube diameter. It seems that the prediction performance

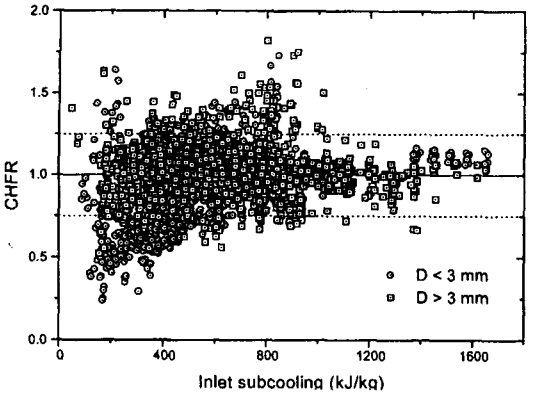

Fig. 11. CHFR vs Inlet Subcooling

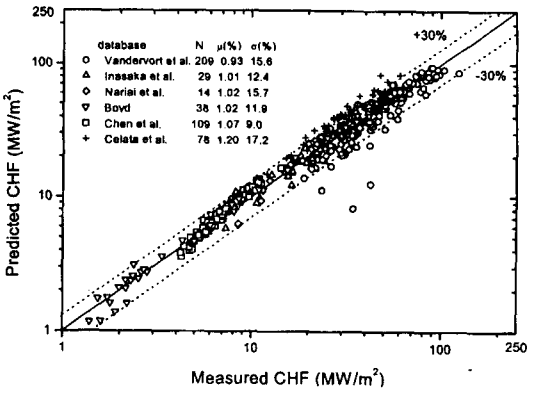

Fig. 13. Predicted vs Measured CHF for Selected Data Sets

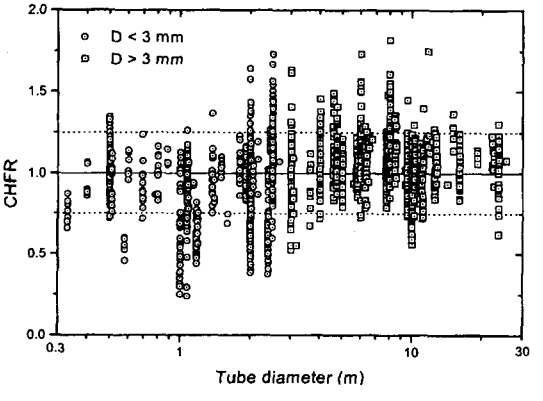

Fig. 12. CHFR vs Tube Diameter

by the Celata et al. model is not sensitive to the tube diameter compared to the authors' CHF model. The reason is that the bulk flow properties such as flow quality and void fraction are not directly used in the CHF prediction procedure, because the Celata et al. model is focused on only the liquid sublayer under vapor clot.

Fig. 8 shows a visual comparison of predictions by the Celata et al. model with the present database. The liquid sublayer dryout model by Celata et al., which was derived by rationalizing existing CHF models, is the only reliable mechanistic model applicable to the high-heat-flux subcooled flow boiling condition. The Celata et al. model is characterized by the absence of empirical constants; however, the model is not free from empiricism even though it does not include a directly fitted constant, because it employs the empirical correlations for the vapor blanket equivalent diameter and the drag coefficient. About 89% of the data points were predicted within ±30%, with μ = 0.91, *RMS* = 19.0%, and σ = 16.4%. The model has a tendency to underpredict the CHF data for the present database. It should be noted that the Celata et al. model was developed using the ENEA CHF database in Table 1.

The proposed model employing the mechanistic method predicted about 89% of the 2938 data points within ±30%, with μ = 1.00, RMS = 18.4%, and σ = 18.4%. Even though one empirical correlation of Eq. (3) was used, this statistical result of prediction performance is acceptable, considering the wide application ranges of the proposed CHF model. Although many data points of the present database in Table

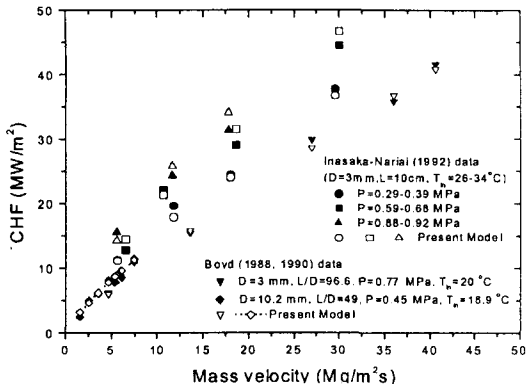

Fig. 14. CHF vs Mass Velocity

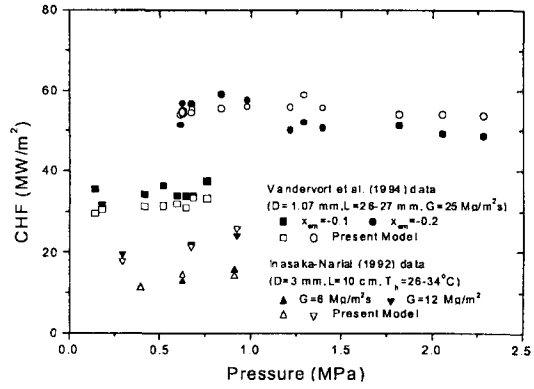

Fig. 15. CHF vs Pressure

1 are out of the applicable range of Eq. (3), the authors' model predicted the CHF with relatively good statistical results for high-heat-flux subcooled flow boiling.

The dependence of the prediction accuracy (CHFR) on major parameters is presented in Fig. 9 through Fig. 12, where the CHFR is plotted versus pressure, mass flux, inlet subcooling, and tube inside diameter, respectively. The comparison of the predictions by the CHF model with experimental data exhibited systematic deviations for the small diameter tube region. For particular, the model has a tendency to underpredict CHF for low pressure ($P < 0.6$ MPa) and low inlet subcooling conditions. For the region of $D \geq 3$ mm, the model underpredicts within a $\pm 25\%$ error band for a low mass flux less than about 2 Mg/m^2s.

The recent CHF data sets of Chen et al. [23], Boyd [24-26], Nariai et al. [27], Inasaka-Nariai [30], Vandervort et al. [31], and Celata et al. [32] were specially selected for the assessment of the proposed model. The data of Vandervort et al., Inasaka-Nariai, and Boyd are included in the ENEA database. Fig. 13 shows the comparison results of prediction by the proposed model.

3.4. Parametric Trends

Figs. 14-18 show the parametric trends of high-heat-flux subcooled flow boiling on the various ranges of pressure, mass velocity, subcooling and tube geometry. An ideal analysis for parametric trend requires that other parameters be kept constant while varying the specific parameter. Unfortunately, it is difficult to find the data sets satisfying such condition. In this parametric trend study, most of the experimental data were obtained from the sources of Vandervort et al.. Fig. 14 shows the influence of mass velocity on CHF in the relatively low pressure regions of 0.3-0.9 MPa, and the present model well predicts the experimental trend of CHF data carried out by Boyd [24, 26] and Inasaka-Nariai [30]. As shown in the figure, the CHF is an increasing function of the mass velocity in the subcooled region, and the trend agrees with general understanding regarding the CHF characteristics.

Fig. 15 shows the effect of pressure on CHF. The CHF seems to be independent of pressure on the data of Vandervort et al., while it slightly increases with an increase in pressure on the data of Inasaka and Nariai. It is known that the CHF

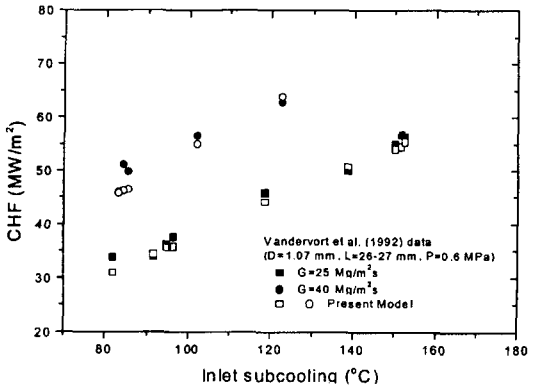

Fig. 16. CHF vs Inlet Subcooling

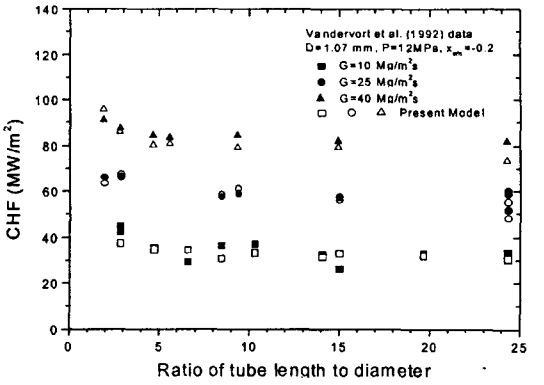

Fig. 18. CHF vs Tube Length-to-Diameter

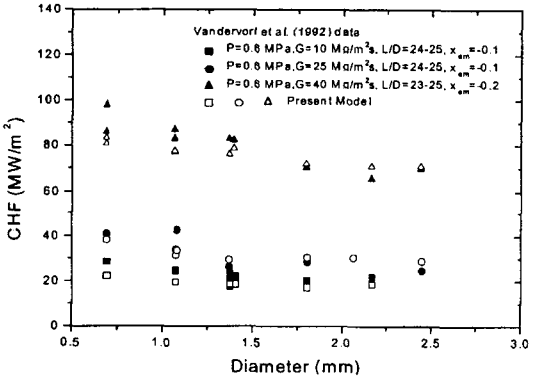

Fig. 17. CHF vs Tube Diameter

for lower and intermediate subcoolings are clearly dependent on the pressure, while those for high subcooling are almost independent of the pressure. Although pressure has a negligible or slight influence on CHF for highly subcooled boiling, the increase of pressure enhances the CHF from a physical viewpoint because higher pressure increases the subcooling degree if other variables are kept constant. The effect of liquid subcooling on CHF is shown in Fig. 16, where CHF increases with an increasing degree of subcooling because the subcooled liquid flow condenses steam bubbles and suppresses their coalescence on the wall.

The effect of tube diameter on CHF is predicted by the present model in Fig. 17. The CHF increases with an increasing tube diameter at fixed inlet conditions, but the effect is less significant for decreased mass velocity. The ratio of the heated length to the tube diameter (L/D) is the characteristic non-dimensional length for the CHF investigation. The present model follows the general trends of experimental data well, as shown in Fig. 18. The CHF increases as L/D decreases, and the length effect has a small contribution to CHF for longer tubes. It is a general understanding that CHF is a decreasing function of tube length for fixed inlet conditions. The parametric trends shown in Figs. 14-18 demonstrate that the present model provides reliable accuracy in predicting independent CHF variations with respect to mass flux, pressure, inlet subcooling, tube diameter, and tube length.

4. Conclusions

A mechanistic CHF model applicable to LWR,

previously developed by the authors, was extended to predict the CHF in the highly subcooled flow boiling, especially for fusion rector components. In order to take into account the enhanced condensation due to high subcooling and high mass velocity in small diameter tubes, a mechanistic approach was adopted to evaluate the non-equilibrium flow quality and void fraction in the subcooled water flow boiling, with preserving the structure of the previous CHF model. Comparison of the model predictions against highly subcooled water CHF data showed relatively good agreement over a wide range of parameters: $0.3 \leq D \leq 37.5$ mm, $0.002 \leq L \leq 4$ m, $0.1 \leq P \leq 20$ MPa, $0.37 \leq G \leq 90$ Mg/m^{2}s, $49 \leq \Delta h_{sub,in} \leq 1659$ kJ/kg, and $0.64 \leq q''_{CHF} \leq 228$ MW/m^2. About 89% of data points were predicted within a $\pm 30\%$ error band with RMS = 18.4%, and σ = 18.4%. This statistical result is acceptable, considering the wide application ranges of the proposed CHF model.

However, a considerable underprediction of the CHF was shown for several data sets with very small diameter tubes (D < 3 mm). The constitutive models employed in the construction of the proposed CHF model might not hold for a small tube diameter at a high mass flux. Taking into account the reduction of void fraction in such extreme conditions, improved theoretical models to evaluate the flow quality and void fraction are required.

Acknowledgements

This work was performed under the Long-term Nuclear R&D Program sponsored by the Korea Ministry of Science and Technology.

Nomenclature

A cross-section area (m^2)
b density ratio defined by Dix
C_p specific heat (J/kg K)
C_o distribution parameter
D tube diameter (m)
D_b detached bubble diameter (m)
f skin friction factor
F_d drag force on a single bubble (N)
G mass flux (kg/m^{2}s), $G_b = \rho_b U_b$, $G_c = \rho_c U_c$
G* limited transverse mixing mass flux (kg/m^{2}s)
g acceleration due to gravity (m/s^2)
h enthalpy (kJ/kg)
Δh degree of subcooling (kJ/kg)
h_s single phase heat transfer coefficient (W/m^{2}K)
h_{fg} latent enthalpy of vaporization (kJ/kg)
k thermal conductivity (W/mK)
P pressure (MPa)
P_H heated perimeter (m)
P_r Prandtl number
q" heat flux (kW/m^2)
Re Reynolds number
U^+ dimensionless velocity
$\overline{U}$ mean velocity (m/s), same as the U_{avg}
v specific volume (m^3/kg)
V_{gj} drift velocity (m/s)
x quality
x_{em} thermal equilibrium quality at tube exit
y distance in radial direction (m)
Y^+ dimensionless distance
Y_B^+ dimensionless distance to tip of vapor bubble
z axial location in flow direction

Greek letters

α void fraction,
β blockage factor
ε roughness size (m)
ε' pumping factor
γ volume quality
η_c fraction of cross-section occupied by core
λ skin friction coefficient

μ viscosity (Ns/m^2)
ρ density (kg/m^3)
σ surface tension (N/m)
τ shear stress (N/m^2)
τ_w apparent wall shear stress (N/m^2)
$\tau_{w,v}$ viscous shear stress on wall (N/m^2)
ξ perimeter (m)

Subscripts

avg average
b bubbly layer or boiling
bc from bubbly layer to core
c core
cb from core to bubbly layer
CHF CHF location
cond condensation
d bubble departure point
f saturated liquid
g saturated vapor
i interface of bubbly layer and core
in inlet
l liquid phase
sub subcooled
w heated wall
2 ϕ two-phase mixture flow

References

1. J. Weisman and B. S. Pei, "Prediction of Critical Heat Flux in Flow Boiling at Low Qualities," Int. J. Heat Mass Transfer **26**, 1463 (1983).
2. C. H. Lee and I. Mudawar, "A Mechanistic Critical Heat Flux Model for Subcooled Flow Boiling Based on Local Bulk Flow Conditions," Int. J. Multiphase Flow **14**, 714 (1988).
3. G. P. Celata., M. Cumo, A. Mariani, M. Simoncini, and G. Zummo, "Rationalization of Existing Mechanistic Models for the Prediction of Water Subcooled Flow Boiling Critical Heat Flux," Int. J. Heat Mass Transfer **37**, suppl.1, 347 (1994).
4. G. P. Celata, M. Cumo, and A. Mariani, "Assessment of Correlations and Models for the Prediction of CHF in Water Subcooled Flow Boiling," Int. J. Heat Mass Transfer **37**, 237 (1994).
5. F. Inasaka and H. Nariai, "Evaluation of Subcooled Critical Heat Flux Correlations for Tubes with and without Internal Twist Tapes," Nucl. Eng. Des. **163**, 225 (1996).
6. Y. M. Kwon and S. H. Chang, "An Improved Mechanistic Model to Predict Critical Heat Flux in Subcooled and Low Quality Forced Convection Boiling," J. Korean Nucl. Society **31**, 236 (1999).
7. Y. M. Kwon and S. H. Chang, "A Mechanistic Critical Heat Flux Model for Wide Range of Subcooled and Low Quality Flow Boiling," Nucl. Eng. Des. **188**, 27 (1999).
8. P. Saha and N. Zuber, "Point of Net Vapor Generation and Vapor Void Fraction in Subcooled Boiling," Proc. 5th Int. Heat Transfer Conf., Tokyo, Japan, Vol. IV, pp.175-179 (1974).
9. F. W. Staub, "The Void Fraction in Subcooled Boiling - Prediction of the Initial Point of Net Vapor Generation," J. Heat Transfer **90**, 151 (1968).
10. S. Levy, "Forced Convection Subcooled Boiling - Prediction of Vapor Volumetric Fraction," Int. J. Heat Mass Transfer **10**, 951 (1967).
11. D. R. H. Beattie and P. B. Whalley, "A Simple Two Phase Frictional Pressure Drop Calculation Method," Int. J. Multiphase Flow **8**, 83 (1982).
12. G. E. Dix, "Vapor Void Fractions for Forced Convection with Subcooled Boiling at Low Flow Rates," NEDO-10491, General Electric Company (1971).

13. O. Styrikovitch, E. I. Nevstrueva, and G. M. Dvorina, "The Effect of Two Phase Flow Pattern on the Nature of Heat Transfer Crisis in Boiling," Proc. 4th Int. Heat Transfer Conf., Paris-Versailles, Vol. VI, pp. B 6.10 (1970).
14. G. P. Celata, "Critical Heat Flux in Subcooled Flow Boiling," Proc. of 11th Int. Heat Transfer Conf., Kyongju, Korea, Vol.1, pp.261- 277 (1998).
15. H. Nariai and F. Inasaka, "Critical Heat Flux and Flow Characteristics of Subcooled Flow Boiling with Water in Narrow Tubes," O. C. Jones and I. Michiyoshi (Ed), Dynamics of Two-Phase Flows, CRC Press, pp.689-708 (1992).
16. S. Z. Rouhani and E. Axelsson, "Calculation of Void Volume Fraction in the Subcooled and Quality Boiling Region," Int. J. Heat Mass Transfer **13**, 383 (1970).
17. R. W. Bowring, "Physical Model Based on Bubble Detachment and Calculation of Steam Voidage in the Subcooled Region of a Heated Channel," Report HPR-10, Inst. For Atomenergi, Halden, Norway (1962).
18. R. T. Lahey Jr. and F. J. Moody, "The Thermal-Hydraulics of a Boiling Water Nuclear Reactor," American Nuclear Society, 2nd edn., La Grange Park, Illinois, Chapter 5 (1993).
19. O. Levenspiel, "Collapse of Steam Bubbles in Water," Ind. Eng. Chem. 51 (1959).
20. B. Thompson and R. V. Macbeth, "Boiling Water Heat Transfer in Uniformly Heated Round Tubes: A Compilation of World Data with Accurate Correlations," AEEW-R-356 (1964).
21. K. M. Becker and G. Strand et al., "Round Tube Burnout Data for Flow of Boiling Water at Pressure between 30 and 200 bar," Report KTH-NEL-14 (1971).
22. A. Zenkevich, "Analysis and Generalization of Experimental Data on Heat Transfer Crisis Associated with Forced Convection of Cooling Water in Tubes," AECL-Tr-Misc-304 (1974).
23. Y. Chen, R. Zhou, L. Hao, and H. Chen, "Critical Heat Flux with Subcooled Boiling of Water at Low Pressure," 8th Int. Topical Meeting on Nuclear Reactor Thermal-Hydraulics, Kyoto, Japan, Vol.2, pp.958-964 (1997).
24. R. D. Boyd, "Subcooled Water Flow Boiling Experiments under Uniform High Heat Flux Conditions," Fusion Technology **13**, 131 (1988).
25. R. D. Boyd, "Subcooled Water Flow Boiling at 1.66 MPa under Uniform High Heat Flux Conditions," ASME Winter Annual Meeting, HTD Vol.119, pp.91-15 (1989).
26. R. D. Boyd, "Subcooled Water Flow Boiling Transition and the L/D Effect on CHF for a Horizontal Uniformly Heated Tube," Fusion Technology **18**, 317 (1990).
27. H. Nariai, F. Inasaka, and H. Kinoshita, "Critical Heat Flux of Subcooled Flow Boiling with and without Internal Twisted Tape under Circumferentially Non-uniform Heating Condition," Proc. German-Japanese Sympo. On Multiphase Flow, pp.191-205 (1994).
28. S. Y. Ahmad, "Axial Distribution of Bulk Temperature and Void Fraction in a Heated Channel with Inlet Subcooling," Trans. ASME, J. Heat Transfer **92**, 595 (1970).
29. A. P. Ornatskii and L. S. Vinyarskii, "Heat Transfer Crisis in a Forced Flow of Underheated Water in Small-bore Tubes," High Temperature **3**, 400 (1965).
30. F. Inasaka and H. Nariai, "Critical Heat Flux of Subcooled Flow Boiling for Water in Uniformly Heated Straight Tubes," Fusion. Eng. Des. **19**, 329 (1992).
31. C. L. Vandervort, A. E. Bergles, and M. K.

Jensen, "An Experimental Study of Critical Heat Flux in Very High Heat Flux Subcooled Boiling," Int. J. Heat Mass Transfer **37**, 161 (1994).

32. G. P. Celata, M. Cumo, and A. Mariani, "Burnout in Highly Subcooled Water Flow Boiling in Small Diameter Tubes," Int. J. Heat Mass Transfer **36**, 1269 (1993).

Appendix I

CHF Calculation Procedure

Required input parameters : D, L, P, G, $\Delta h_{sub,in}$ (or h_{in}).

(1) Assume a value for q".

(2) Calculation of $\Delta h_{sub,d}$ where all physical properties are calculated at saturated state at the system pressure.

$$Y_B^+ = 0.015\frac{(\sigma_f D\rho_f)^{1/2}}{\mu_f}$$

$$\text{if } 0 \le Y_B^+ \le 5,\quad \Delta h_{sub,d} = q''\left[\frac{C_{pf}}{h_s} - \frac{\mathrm{Pr}_f Y_B^+}{G\sqrt{f/8}}\right]$$

$$\text{if } 5 < Y_B^+ \le 30,\quad \Delta h_{sub,d} = q''\left[\frac{C_{pf}}{h_s} - \frac{5}{G\sqrt{f/8}}\left[\mathrm{Pr}_f + \ln\left(1+\frac{\mathrm{Pr}_f Y_B^+}{5} - \mathrm{Pr}_f\right)\right]\right]$$

$$\text{if } Y_B^+ > 30,\quad \Delta h_{sub,d} = q''\left[\frac{C_{pf}}{h_s} - \frac{5}{G\sqrt{f/8}}\left[\mathrm{Pr}_f + \ln(1+5\mathrm{Pr}_f) + \frac{1}{2}\ln\left(\frac{Y_B^+}{30}\right)\right]\right]$$

where

$$f = 0.0055\left[1+\left(20000\frac{\varepsilon}{D}+\frac{10^6}{\mathrm{Re}_f}\right)^{1/3}\right] \quad \text{with } \varepsilon/D = 10^{-4}$$

$$h_s = 0.023\mathrm{Re}_f^{0.8}\mathrm{Pr}_f^{0.4}(k_f/D) \text{ with } \mathrm{Re}_f = \frac{GD}{\mu_f} \text{ and } \mathrm{Pr}_f = \frac{C_p\mu_f}{k_f}$$

(3) Calculation of x_d and z_d.

$$x_d = \frac{-\Delta h_{sub,d}}{h_{fg}}, \qquad z_d = \frac{GD(h_f - \Delta h_{sub,d} - h_{in})}{4q''}, \qquad h_d = h_f - \Delta h_{sub,d}$$

$$\text{if } z_d < 0; z_d = 0 \text{ and } x_d = \frac{-\Delta h_{sub,in}}{h_{fg}}$$

(4) Calculation of x_{avg} and α_{avg} at the tube exit (iterative calculation of x_{avg})

$$h_l = \frac{h_{avg} - h_g x_{avg}}{1-x_{avg}} \quad \text{with } h_{avg} = h_{in} + \frac{4q''L}{GD}$$

$$T_l = T(P,h_l),\quad \rho_l = \rho(P,h_l),\quad \sigma_l = \sigma(T_l),\quad \mu_l = \mu(\rho_l,T_l)$$

$$\alpha_{avg} = \frac{x_{avg}}{\left\{C_o\left[x_{avg} + \frac{\rho_g}{\rho_l}(1-x_{avg})\right] + \frac{\rho_g V_{gj}}{G}\right\}}$$

where

$$C_o = \gamma\left[1+\left(\frac{1}{\gamma}-1\right)^b\right] \quad \text{with } \gamma = \frac{x_{avg}}{\left[x_{avg} + \frac{\rho_g}{\rho_l}(1-x_{avg})\right]} \text{ and } b = \left(\frac{\rho_g}{\rho_l}\right)^{0.1}$$

$$V_{gj} = 2.9\left[\frac{(\rho_l-\rho_g)\sigma_l g}{\rho_l^2}\right]^{1/4}$$

$$\rho_{avg} = \frac{\alpha_{avg}\rho_g}{x_{avg}}, \qquad \varepsilon' = \frac{\rho_l(h_f - h_l)}{\rho_g h_{fg}}$$

$$q''_{cond} = 0.075\frac{h_{fg}D\alpha_{avg}}{4v_{fg}}(T_{sat}-T_l) \text{ for } h_l \ge h_d, \quad q''_{cond} = 0 \text{ for } h_l < h_d$$

$$q''_b = q''\frac{h_l - h_d}{h_f - h_d} \text{ for } h_l \ge h_d, \quad q''_b = 0 \text{ for } h_l < h_d$$

$$x_{avg} = \frac{4(L-z_d)}{GDh_{fg}}\left(\frac{q''_b}{1+\varepsilon'} - q''_{cond}\right)$$

(5) Calculation of D_b.

$$\mu_{2\phi} = \mu_f(1-\alpha_{avg})(1+2.5\alpha_{avg}) + \mu_g\alpha_{avg}, \quad \mathrm{Re}_{2\phi} = \frac{GD}{\mu_{2\phi}}, \quad f_{2\phi} = f(\mathrm{Re}_{2\phi})$$

$$D_b = 0.015\sqrt{\frac{8\sigma_f D\rho_{avg}}{f_{2\phi}G^2}}$$

(6) Calculation of flow properties at the tube exit

$$\eta_c = \left(\frac{D-2D_b}{D}\right)^2$$

$$\alpha_b = 0.83 - 0.29\exp(-4.71x_{em} - 1.89), \quad \alpha_c = \frac{1}{\eta_c}\alpha_{avg} - \frac{1-\eta_c}{\eta_c}\alpha_b$$

$$\rho_b = \rho_f(1-\alpha_b) + \rho_g\alpha_b, \qquad \rho_c = \rho_l(1-\alpha_c) + \rho_g\alpha_c$$

$$x_b = \frac{\alpha_b\rho_g}{\rho_b}, \quad x_c = \frac{\alpha_c\rho_g}{\rho_c}, \quad h_b = h_f(1-x_b) + h_g x_b, \quad h_c = h_l(1-x_c) + h_g x_c$$

(7) Calculation of average velocities

$$\frac{1}{\sqrt{\lambda}} = 3.48 - 4\log\left(\frac{2D_b}{D} + \frac{9.35}{\mathrm{Re}_{2\phi}\sqrt{\lambda}}\right), \quad \tau_w = \frac{\lambda G^2}{2\rho_c\eta_c^2}, \quad Y^+ = \frac{D_b\sqrt{\tau_w\rho_c}}{\mu_{2\phi}}$$

$$\text{if } 0 \le Y^+ < 5,\quad \overline{U}_b = 0.5Y^+\sqrt{\frac{\tau_w}{\rho_c}}$$

$$\text{if } 5 \le Y^+ < 30,\quad \overline{U}_b = 0.5(5\ln Y^+ - 3.05)\sqrt{\frac{\tau_w}{\rho_c}}$$

$$\text{if } Y^+ \ge 30,\quad \overline{U}_b = 0.5(2.5\ln Y^+ + 5.5)\sqrt{\frac{\tau_w}{\rho_c}}$$

$$\overline{U}_c = \frac{G - \overline{U}_b\rho_b(1-\eta_c)}{\rho_c\eta_c}$$

(8) Calculation of q''_{CHF}

$$F_d = \frac{\lambda \rho_c \bar{U}_c^2}{2}\left(\frac{\pi D_b^2}{4}\right)$$

$$\xi_w = \pi D, \quad \xi_i = \pi(D - 2D_b)$$

$$G^* = \left[-(\rho_c - \rho_b)g + \frac{\pi D F_d}{D_b^2(1-\eta_c)A}\right]\frac{A\eta_c(1-\eta_c)}{(\bar{U}_c - \bar{U}_b)\xi_i}$$

$$q''_{CHF} = G^*(h_b - h_c)\frac{\xi_i}{\xi_w}$$

If the estimated q'' in step (1) is close enough to the calculated q''_{CHF} in step (8), q'' is the critical heat flux. Otherwise, readjust q'' and return to step (1).